ADVANCED FUNCTIONAL MATERIALS
www.afm-journal.de

Magnetic-Field Controllable Displacement-Type Ferroelectricity Driven by Off-Center Fe^{2+} Ions in $CaFe_3Ti_4O_{12}$ Perovskite

*Dabiao Lu, Denis Sheptyakov, Yingying Cao, Haoting Zhao, Jie Zhang, Maocai Pi, Xubin Ye, Zhehong Liu, Xueqiang Zhang, Zhao Pan, Xingxing Jiang, Zhiwei Hu, Yi-feng Yang, Pu Yu, and Youwen Long**

Displacement-type ferroelectrics usually exclude magnetic *d*-electron contribution. Applying a magnetic field thus can little change the electric polarization. Herein, a magnetic ionic driven displacement-type perovskite ferroelectric $CaFe_3Ti_4O_{12}$ is reported. In this compound, magnetic Fe^{2+} ions contribute to both ferroelectric and antiferromagnetic orders respectively at T_C ≈107 and T_N ≈ 3.1 K, resulting in coupled electric and magnetic domains. A moderate magnetic field can induce a metamagnetic transition toward ferromagnetic correlations. External magnetic fields can thus readily tune the magnetic and the joint ferroelectric domains, giving rise to exceptional magnetic-field controllable displacement-type polarization with a large magnetoelectric (ME) coupling coefficient. This study opens up a new avenue to find unprecedented ME effects in displacement-type ferroelectrics for numerous applications.

1. Introduction

Displacement-type perovskite ferroelectrics, such as $BaTiO_3$, $PbTiO_3$, and $Pb(Zr_{1-x}Ti_x)O_3$, have received much attention owing to their superior performance and various practical applications in capacitors, sensors, and actuators.[1–3] Since nonmagnetic d^0 and lone-pair $6s^2$ ions are usually responsible for displacive ferroelectric (FE) distortions,[4–6] applying an external magnetic field cannot effectively change the magnitude of electric polarization (*P*). Even though some magnetic ions coexist with the displacive d^0 or $6s^2$ ions as reported in $BiFeO_3$,[7] $BiMnO_3$,[8] $PbFe_{0.5}Nb_{0.5}O_3$[9] etc, ferroelectricity and magnetism originate from different cations. As a result, the *P* is almost independent on magnetic field.[10–12] It is thus a substantial challenge to use magnetic fields to control the spontaneous polarization in a displacement-type ferroelectric.

If magnetic *d*-electrons in a solid can not only displace directionally but also form a peculiar spin order with sensitive magnetic field dependence, such a peculiar material may provide a unique opportunity to realize strong magnetic-field controllable displacement-type ferroelectricity. Unfortunately, this case is extremely rare to occur.[4] For example, although displacive magnetic ions are involved in $YMnO_3$,[13] $Sr_{1-x}Ba_xMnO_3$ ($0.45 < x < 0.5$),[14] and $Ca_3Mn_2O_7$,[15] the robust antiferromagnetic (AFM) order (i.e., the AFM

D. Lu, Y. Cao, H. Zhao, J. Zhang, M. Pi, X. Ye, Z. Liu, X. Zhang, Z. Pan, Y.-feng Yang, Y. Long
Beijing National Laboratory for Condensed Matter Physics
Institute of Physics
Chinese Academy of Sciences
Beijing 100190, China
E-mail: ywlong@iphy.ac.cn

D. Lu, Y. Cao, H. Zhao, J. Zhang, M. Pi, Y.-feng Yang, Y. Long
School of Physical Sciences
University of Chinese Academy of Sciences
Beijing 100049, China

D. Sheptyakov
Laboratory for Neutron Scattering and Imaging (LNS)
Paul Scherrer Institut (PSI)
Forschungsstrasse 111, Villigen CH-5232, Switzerland

X. Jiang
Technical Institute of Physics and Chemistry
Chinese Academy of Sciences
Beijing 100190, China

Z. Hu
Max Planck Institute for Chemical Physics of Solids
01187 Dresden, Germany

Y.-feng Yang, Y. Long
Songshan Lake Materials Laboratory
Dongguan, Guangdong 523808, China

P. Yu
State Key Laboratory of Low Dimensional Quantum Physics and Department of Physics
Tsinghua University
Beijing 100084, China

The ORCID identification number(s) for the author(s) of this article can be found under https://doi.org/10.1002/adfm.202411133

DOI: 10.1002/adfm.202411133

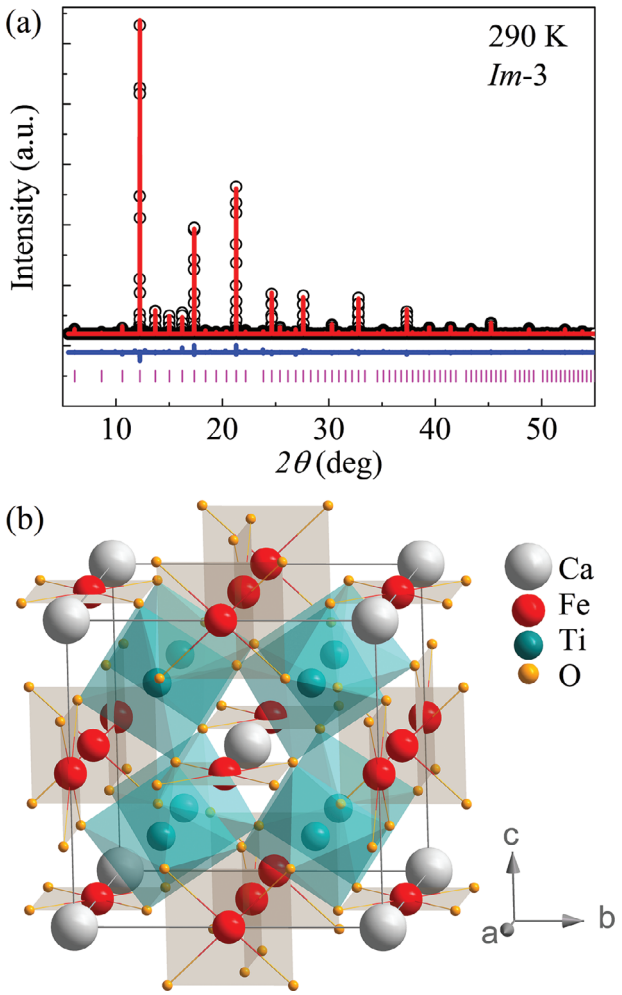

Figure 1. a) Rietveld refinement results based on the SXRD data collected at 290 K for $CaFe_3Ti_4O_{12}$. Observed (black circles), calculated (red line), and difference (blue line) are illustrated, respectively. The magenta ticks indicate the allowed Bragg reflections of space group *Im*-3. b) Schematic of the crystal structure of CFTO in its *Im*-3 symmetry.

structure is unchanged by magnetic field) formed in these ferroelectrics hinders the presence of magnetic-field controllable polarization.[15–17] Herein, we report an exceptional magnetic Fe^{2+} ions driven displacement-type ferroelectric $CaFe_3Ti_4O_{12}$ (CFTO). In sharp contrast to the above compounds, external magnetic fields can readily tune the AFM structure toward ferromagnetic (FM) correlations. Consequentially, applying magnetic fields can readily change the magnetic domains and the coupled FE domains, giving rise to significant magnetic-field controllable displacement-type ferroelectricity in CFTO.

2. Results and Discussion

Figure 1a shows the synchrotron x-ray diffraction (SXRD) pattern of CFTO collected at 290 K and the relative Rietveld refinement results. All the diffraction peaks can be indexed to A-site ordered $AA'_3B_4O_{12}$-type quadruple perovskite structure with space group *Im*-3 (No. 204), and no visible impurity phase was present. In this symmetry, Ca and Fe are completely ordered at the Wyckoff positions 2*a* (0, 0, 0) and 6*b* (0, 0.5, 0.5), due to the large ionic size difference, whereas Ti and O occupy positions 8*c* (0.25, 0.25, 0.25) and 24 *g* (*x*, *y*, 0), respectively. The refined structural parameters are listed in Table S1 (Supporting Information). Satisfactory goodness-of-fit parameters were obtained, as characterized by R_p = 2.19% and R_{wp} = 3.23%. Both bond valence sum calculations and x-ray absorption spectroscopy results confirmed the charge combination to be $Ca^{2+}Fe^{2+}{}_3Ti^{4+}{}_4O_{12}$ (see Table S1 and Figure S1, Supporting Information). Figure 1b depicts the schematic of the crystal construction of CFTO in its *Im*-3 symmetry. Corner-sharing TiO_6 octahedra are formed for the B-site Ti^{4+}, while square-planar coordinated FeO_4 units appear for the A′-site magnetic ions of Fe^{2+}.

Figure 2a shows the temperature dependence of magnetic susceptibility (χ) for CFTO measured at 0.1 T. As the temperature decreased to $T_N \approx 3.1$ K, a sharp cusp was observed in both the zero-field-cooling (ZFC) and field-cooling (FC) susceptibility curves, indicating the occurrence of an AFM phase transition. Above 50 K, the data of χ^{-1} can be well fitted using the Curie–Weiss law with the function $\chi^{-1} = (T - \theta) / C$ (see Figure S2, Supporting Information). Figure 2b shows the isothermal magnetization curves between −7 and 7 T. The linear magnetization behavior observed above T_N (e.g., 100 K) is in accordance with paramagnetism. Below T_N, such as at 2 K, one can find a metamagnetic transition (see the inset for clarity) from the initial AFM state with linear magnetization to a ferromagnetism-like state with a magnetic moment of 8.5 μ_B f.u.$^{-1}$ up to 7 T. Even at temperatures considerably higher than T_N such as at 10 K, field-induced FM behavior still exists. Based on the temperature dependent magnetization measured at different fields (see Figure 2c), one finds that the AFM cusp gradually disappears with the field increasing to a critical value $H_C \approx 0.8$ T, and higher fields can induce FM correlations at temperatures well above T_N. These results reveal the readily tunable spin alignment of CFTO in magnetic fields.

Corresponding to the AFM phase transition, a sharp λ-type anomaly occurred in the specific heat (C_p) at T_N (refer to Figure 2d and the inset), suggesting the second-order nature of the AFM transition. Unexpectedly, the C_p curve displayed a second anomaly, which was rather broad near 110 K. Because no magnetic variation occurs around this temperature, the relative dielectric constant ϵ_r(T) was measured to examine the origin of this anomaly. As shown in **Figure** 3a, ϵ_r(T) displays a sharp peak at the critical temperature $T_C \approx 107$ K. Moreover, the position of the dielectric peak is completely frequency independent, implying a possible FE phase transition. Below T_C, CFTO exhibits quite low dielectric loss ($tan\delta < 0.05$) as shown in Figure 3b. Far above T_C (e.g., > 170 K), the dielectric loss, especially at lower frequencies, increases with increasing temperature, indicating the presence of some leakage effects, which could make the magnitude of ϵ_r(T) change somewhat above T_C at different frequencies. Note that $tan\delta$ does not show a similar frequency-independent peak as ϵ_r(T) does at T_C. This may be attributed to grain-size effects as reported elsewhere.[18] Near T_N, ϵ_r(T) shows a tiny downturn (see the inset for clarity). This feature was also observed in some hexagonal FE manganites[19] owing to the decrease of the polar ionic displacement during the AFM phase transition, i.e, a magneto-elastic coupling effect.[20] Moreover, magnetic fields can

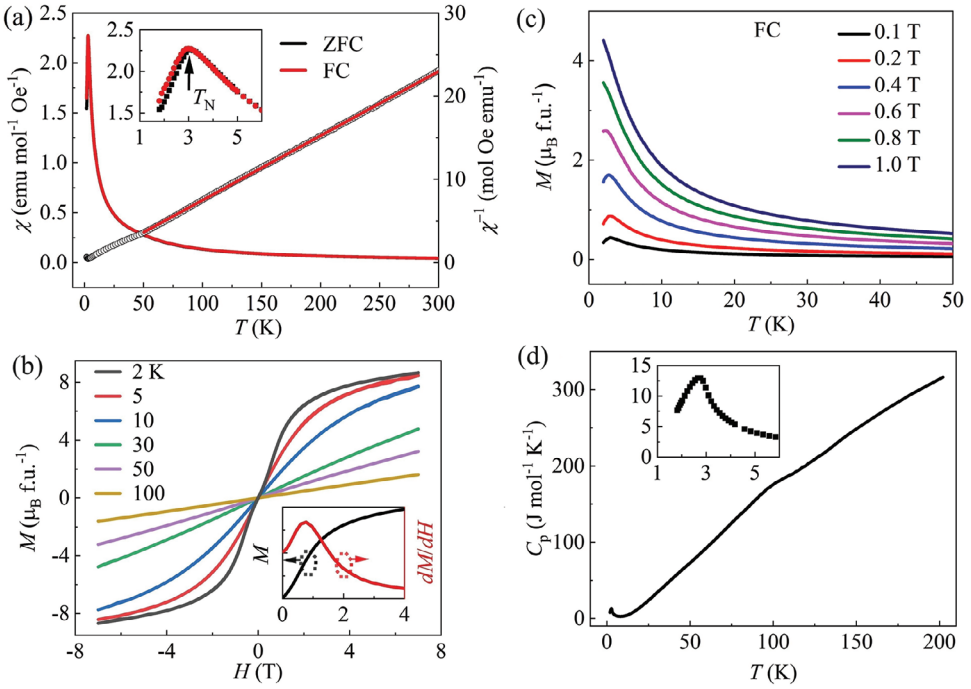

Figure 2. a) Temperature dependence of magnetic susceptibility χ measured at 0.1 T using ZFC and FC modes (left axis), and the Curie–Weiss fitting (blue line) for the ZFC data of χ^{-1} above 50 K (right axis). The inset shows the enlarged view for the AFM transition. b) Magnetic field dependence of magnetization measured at some fixed temperatures. The inset shows the derivative of magnetization to characterize the metamagnetic transition. c) Temperature dependence of magnetization measured at different magnetic fields. d) Temperature dependence of specific heat C_p. The inset shows the anomaly associated with the AFM transition.

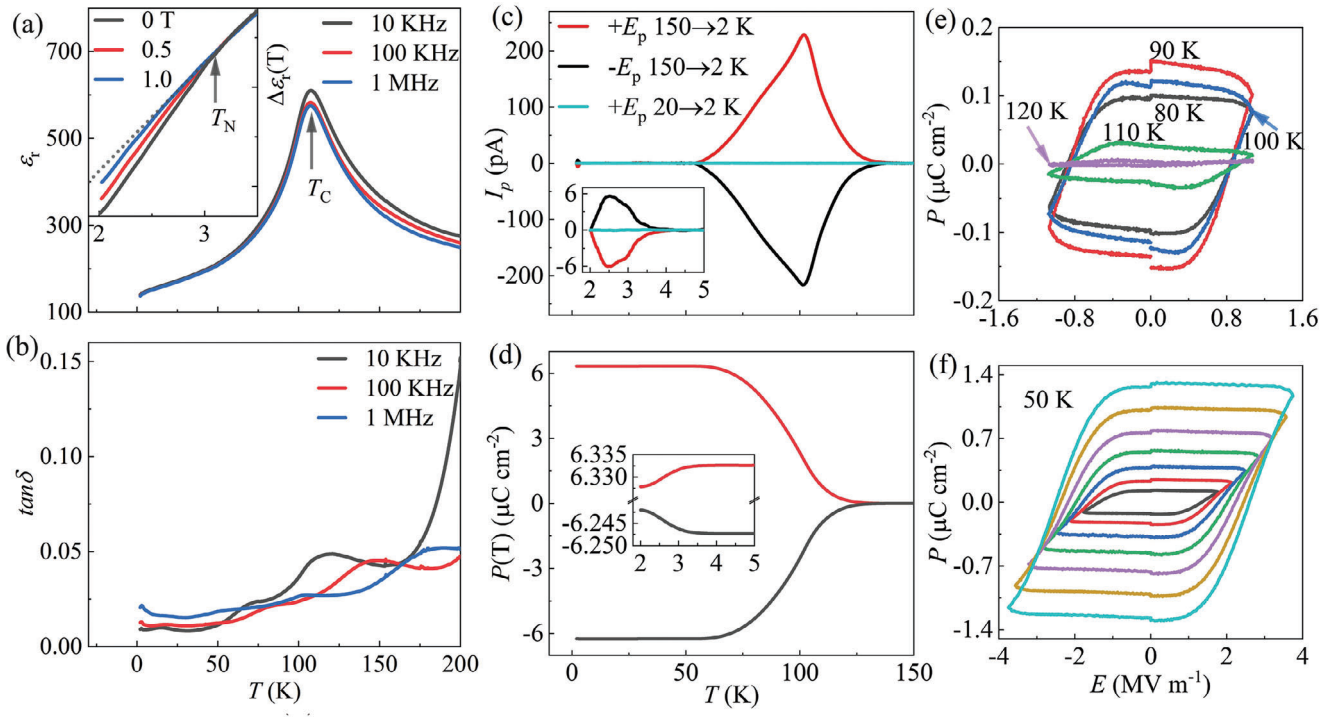

Figure 3. Temperature dependence of a) relative dielectric constant ϵ_r, b) dielectric loss *tanδ* measured at different frequencies, c) pyroelectric current I_p(T) measured under different poling procedures with the value of the poling field E_p = 1.0 MV m^{-1}, d) electric polarization P(T) by integrating the pyroelectric currents poled from 150 to 2 K. The inset in (a) shows $\Delta\epsilon_r(T) = \epsilon_r(T) - \epsilon_r(5\ K)$ measured at 10 KHz and different magnetic fields. And the dotted line is the linear extension of $\Delta\epsilon_r$(T) curve at T_N. The insert in (c,d) shows the enlarged view for I_p(T) and P(T) near T_N, respectively. Ferroelectric hysteresis loops measured e) at selected temperatures with excitation electric fields $E \approx$ 1.0 MV m^{-1}, f) at 50 K with different excitation electric fields.

suppress the dielectric down-turn at T_N in CFTO, in accordance with the readily tunable AFM state.

To confirm the FE phase transition occurring at T_C, the temperature dependent pyroelectric current I_p(T) was measured after poling the sample from 150 to 2 K, and then the related P(T) was obtained for CFTO by integrating the I_p(T) as a function of time. As shown in Figure 3c, a sharp pyroelectric peak is observed near T_C, where P(T) experiences a remarkable increase (Figure 3d). Moreover, both I_p(T) and P(T) are reversible if the sign of the poling electric field (E_p) changes from positive to negative, demonstrating the occurrence of an FE transformation at T_C. Note that the value of P (6.4 μC cm^{-2}) is not saturated under this E_p (1.0 MV m^{-1}), since P increases with increasing poling fields as shown in Figure S3 (Supporting Information). In addition, by using the aforementioned poling process from 150 to 2 K, a small pyroelectric peak is found to occur at T_N, which has an opposite sign to that observed at T_C (see the inset of Figure 3c). To check whether this small anomaly is an independent electric polarization caused by the AFM order of Fe^{2+} or not, the I_p(T) was also measured by poling the sample from 20 to 2 K with E_p only across T_N, but not T_C. In this procedure, however, no pyroelectric and polarization variation occur at T_N (see the inset of Figure 3c), revealing that the small polarization at T_N is originated from the polarization generated by the FE phase transition at T_C, rather than independently induced by the AFM spin texture. This result is in good agreement with the dielectric down-turn, indicating that the AFM magneto-elastic effect slightly reduces P at T_N.

Since the pyroelectric measurement may contain some extrinsic contributions like thermally stimulated current,[21] FE hysteresis loops were measured to further confirm the ferroelectricity of CFTO by using the positive-up negative-down (PUND) method. This method can exclude extrinsic contributions, such as dielectric and conductive components.[22,23] As illustrated in Figure 3e, at temperatures below T_C, one can find canonical *PE* loops, whereas the P is zero well above T_C (e.g., at 120 K). A small amount of polarization can be observed at 110 K, implying the existence of some short-range FE domains near T_C. At fixed temperatures (e.g., 50 K), the *PE* loops expand with increasing electric field, as shown in Figure 3f. The value of FE polarization increases from 0.026 to 1.30 μC cm^{-2} as the electric field increases from 1.79 to 3.77 MV m^{-1}. Because the sample was broken under higher applied electric fields owing to the leakage effect, one cannot determine the saturated polarization in the polycrystalline CFTO. Note that the magnitude of polarization obtained by *PE* loops (1.30 μC cm^{-2}) is smaller than that obtained by pyroelectric current (6.4 μC cm^{-2}), due to the more readily tuned ferroelectric domains by using pyroelectric poling procedures and some contributions of thermal stimulated currents in pyroelectric measurements. Nevertheless, the temperature dependent polarization and *PE* loops confirmed the occurrence of an intrinsic paraelectricity-to-ferroelectricity phase transition at $T_C \approx 107$ K.

To identify the polar crystal structure of CFTO below T_C, SXRD was performed at different temperatures. As shown in Figure S4a (Supporting Information), one cannot discern any new diffraction peaks or apparent peak splitting in the current resolution. However, if we check the height and width for some diffraction peaks, there are clear variations with temperatures (see Figure S4b–e, Supporting Information). As depicted in Figure S4f (Supporting Information), although the relative intensities of some diffraction peaks remain almost unchanged above T_C, they undergo remarkable divergence at the onset of T_C. Moreover, the gradually decreasing full width at half maximum (FWHM) started to sharply increase with the temperature down to T_C (see Figure S4g, Supporting Information). In addition, similar behavior can also be found in neutron powder diffraction (NPD) patterns (see Figure S5, Supporting Information). These features provide evidence for the occurrence of structural phase transition of CFTO at T_C.

Based on Landau's theory of the symmetry-breaking structure phase transition, the lower-symmetry structure is described by order parameters that are transformed according to the irreducible representation (irrep.) for the space group of the higher-symmetry parent phase.[24] Because no new diffraction peak appears in the SXRD patterns of CFTO, the lattice translations should be maintained in the subgroup. This implies that the wave vector of irrep. is zero, corresponding to point Γ in the Brillouin zone. With the limitation of polar subgroups, irrep. can be further determined to be Γ_4^- only, yielding two possible polar space groups, *R*3 (No. 146) and *Imm*2 (No. 44).[25] Furthermore, these two space groups as well as the high-temperature *Im*-3 were used to refine the SXRD pattern collected at 5 K. As shown in Table S2 (Supporting Information), the *R*3 symmetry gives the most reliable refinement. Similarity, a significant improvement in refinement quality for NPD pattern at 5 K can be achieved by using *R*3 instead of *Im*-3 space group (see Figure S6, Supporting Information). To determine the space group further, first-principles calculations were performed. During the calculations for the ground-state structure, it was found that the *R*3 phase was more energetically favorable than the *Imm*2 phase by 0.63 eV/f.u., suggesting that *R*3 is most probable for the low-temperature polar phase of CFTO (the electronic band structures of *R*3 phase are shown in Figure S7, Supporting Information). Thus, we used space group *R*3 to analyze the SXRD data collected below T_C. **Figure 4a** shows an example of Rietveld refinement based on the SXRD pattern obtained at 5 K, and the detailed structural parameters are listed in Table S3 (Supporting Information). Figure 4b shows the temperature dependence of the lattice constants and unit cell volumes of CFTO. The paraelectric and ferroelectric phases exhibited different temperature dependences, but the cell volume experienced only a slight variation at T_C.

Figure 4c shows a schematic of the crystal structure of the polar rhombohedral FE phase. This polar structure was formed by slightly shortening the initial cubic *Im*-3 structure along the[1 1 1] direction. Accompanying the structural phase transition from *Im*-3 to *R*3, the initially single Ti position separates into two different Wyckoff positions, that is, 3*a* (0, 0, *z*) for Ti1 and 9*b* (*x*, *y*, *z*) for Ti2, whereas Fe occupies a single Wyckoff position of 9*b*. Both Ti and Fe are displaced from the polyhedral centers, resulting in displacement-type FE polarization. Restricted by the symmetry of *R*3, the displacement direction of Ti1 is along the *c* axis. For Ti2 and Fe, the *ab*-plane displacive effects cancel out, leading to the net displacement along the *c*-axis direction, too. Figure 4d illustrates the magnitude of displacements for Ti and Fe ions. Specifically, Ti1 and Ti2 are displaced from the original position of the cubic phase by 0.03 and 0.07 Å, respectively. The displacement of Fe is 0.15 Å, which is much larger than those of Ti, suggesting that the square-coordinated Fe plays an important role for the formation of displacement-type FE polarization of CFTO. Based

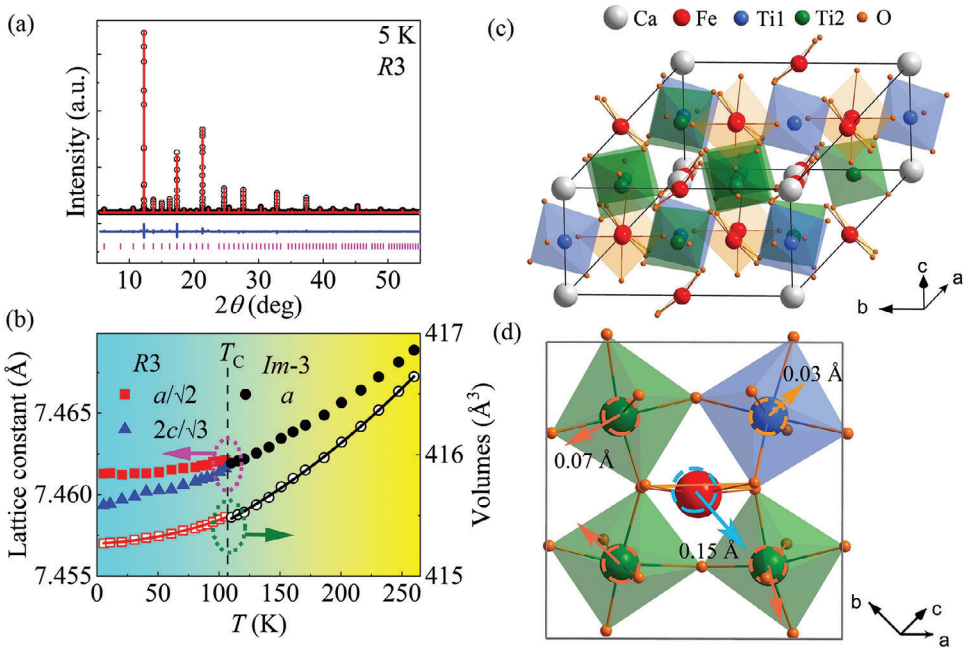

Figure 4. a) Rietveld refinement results based on the SXRD data collected at 5 K using the *R*3 space group. Observed (black circles), calculated (red line), and difference (blue line) are illustrated. The magenta ticks indicate the allowed Bragg reflections. b) Temperature dependence of lattice constants and cell volume. The solid curves show the distinct tendencies of the cell volumes by fitting the data with quadratic polynomials. c) Schematic of the crystal structure of CFTO in its *R*3 symmetry. d) Ionic displacements in the polar rhombohedral phase. The square cell edge and dotted cycles represent the cell edge and cations' positions in the cubic phase, respectively. The arrows illustrate the displacive directions with the distances shown nearby.

on the point charge model, the value of net spontaneous electric polarization arising from the cations' displacements is calculated as 36.9 μC cm^{-2}, which is comparable with those for some canonical ferroelectrics, such as $BaTiO_3$ (26 μC cm^{-2}).[26]

To further elucidate the driving force for the FE transition of CFTO, we summarized currently reported $AA'_3B_4O_{12}$-type perovskite compounds[27–31] with Ti^{4+} at B-site in **Table 1**. Since a small tolerance factor $t = (r_A + r_O)/\sqrt{2}(r_B + r_O)$ (r_A, r_B, & r_O represent for the ionic radius of A, B, and O, respectively) is generally incompatible with d^0 ions induced ferroelectricity in a perovskite structure,[32,33] most compounds in Table 1 are nonpolar, with the exception of $PbHg_3Ti_4O_{12}$ and CFTO. Considering the nonpolar nature of $SrHg_3Ti_4O_{12}$, one can deduce that the ferroelectricity of $PbHg_3Ti_4O_{12}$ is primarily driven by the $6s^2$ lone-pair electrons of Pb^{2+} ions. However, CFTO does not possess $6s^2$ ions, one can thus infer that the unique Fe^{2+} ions play a crucial role for the FE transition of CFTO.

Table 1. Currently reported $AA'_3B_4O_{12}$-type perovskite oxides with Ti^{4+} at B-site.

Compounds	tolerance factor	$6s^2$ ions	ferroelectricity	Refs.
$CaFe_3Ti_4O_{12}$	0.78	None	107 K	This work
$CaCu_3Ti_4O_{12}$	0.76	None	Nonpolar	[27]
$SrCu_3Ti_4O_{12}$	0.77	None	Nonpolar	[28]
$CaCo_3Ti_4O_{12}$	0.77	None	Nonpolar	[29]
$CaPd_3Ti_4O_{12}$	0.78	None	Nonpolar	[30]
$SrHg_3Ti_4O_{12}$	0.88	None	Nonpolar	[31]
$PbHg_3Ti_4O_{12}$	0.88	Pb^{2+}	250 K	[31]

Because Fe^{2+} ions contribute to both magnetic order and displacement-type ferroelectricity, the polarization is expected to be controlled by applying magnetic fields in CFTO. **Figure 5a** shows the change of polarization $\Delta P(H) = P(H) - P(0\,T)$ as a function of the magnetic field at different temperatures. One finds that the $\Delta P(H)$ monotonically decreases with increasing magnetic field from 0 to 9 T at all temperatures we measured. The absolute value of the $\Delta P(H)$ is as large as 0.1 μC cm^{-2} at 2 K and 9 T. Even at 30 K, this value reaches 0.05 μC cm^{-2}. Based on field dependent polarization, we can calculate the magnetoelectric (ME) coupling coefficient α by the formula $\alpha = dP/dH$. As shown in Figure 5b, an unexpectedly large α value of up to 500 ps m^{-1} is observed at 2 K and 0.8 T for CFTO. It is well known that in conventional displacement-type ferroelectrics, the magnetic field has little effect on the magnitude of polarization.[11,12,34] In comparison, the α coefficient of CFTO is even comparable to those observed in some typical type-II multiferroics,[11] where the P is induced by peculiar spin textures instead of ionic displacements, such as $TbMn_2O_5$ ($\alpha \approx 500$ ps m^{-1} at 1 T),[35] $TbMnO_3$ ($\alpha \approx 250$ ps m^{-1} at 4.5 T),[36] and $Ni_3V_2O_8$ ($\alpha \approx 500$ ps m^{-1} at 1.7 T).[37] However, because the value of spin-induced polarization is usually extremely small, the field-tunable magnitude of $\Delta P(H)$ in these type-II multiferroics (0.08, 0.04, and 0.013 μC cm^{-2} for $TbMn_2O_5$, $TbMnO_3$, and $Ni_3V_2O_8$, respectively) is much lower than that detected in the current CFTO.

To explore the origin of the large $\Delta P(H)$ in CFTO, $\Delta P(H)$ was measured by using different poling procedures, including the poling field E_p just across T_N (from 20 to 2 K) and T_C (from 150

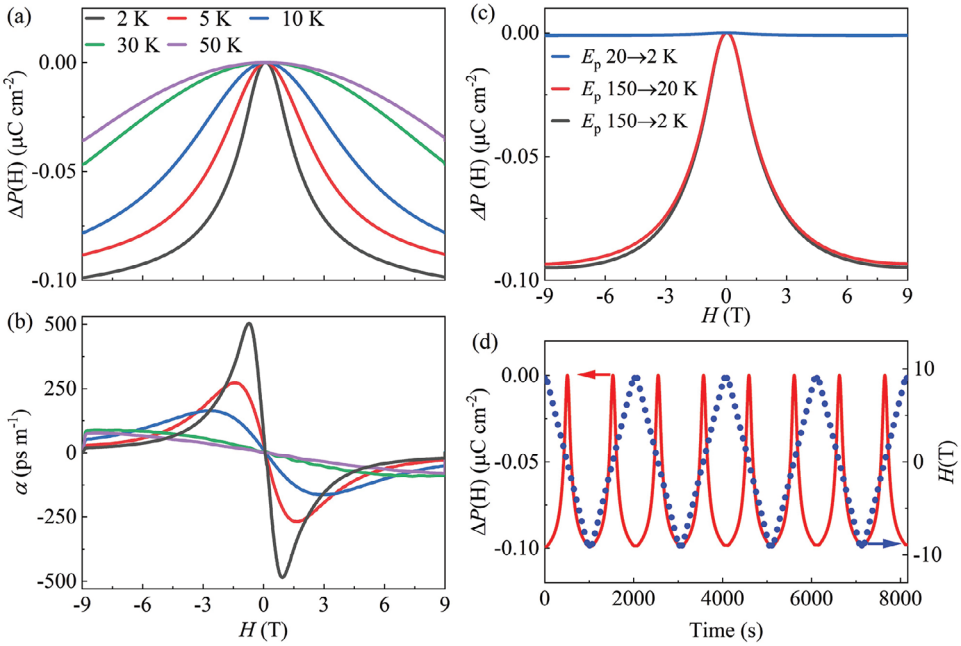

Figure 5. Magnetic field as a function of, a) change of electric polarization $\Delta P(H) = P(H) - P(0\ T)$, b) magnetoelectric coupling coefficient $\alpha = dP / dH$ for CFTO. Before measurement of $\Delta P(H)$ in (a), the sample was poled from 150 to 2 K with poling field $E_p = 1$ MV m^{-1}. c) Field dependence of $\Delta P(H)$ measured at 2 K using different poling procedures. d) Repeatable change of electric polarization (red line) under a triangularly periodic magnetic field (blue dotted line) measured at 2 K.

to 20 K) as well as E_p across both T_C and T_N (from 150 to 2 K). As shown in Figure 5c, no obvious $\Delta P(H)$ can be observed with E_p just across T_N (the first procedure), whereas significant $\Delta P(H)$ occurs as long as the polarization associated with Fe^{2+} displacement is aligned by a poling field (the last two procedures). These results reveal that the $\Delta P(H)$ arises from the displacement-type FE polarization generated at T_C, while the AFM order at T_N itself does not contribute to ME effects in CFTO.

Note that in magnetic ions involved ferroelectrics, strong coupling between ferroelectric and magnetic order is generally realized. For example, in perovskite $Sr_{1-x}Ba_xMnO_3$ ($0.45 < x < 0.5$),[14] the FE polarization is driven by off-center magnetic Mn^{4+} ions significantly reduces at the AFM phase transition. In double-layered perovskites $Ca_3Mn_2O_7$,[15] the ferroelectricity was induced by tilting of MnO_6 octahedra, and the magnetization can be slightly changed by applying an electric field. And in hexagonal $YMnO_3$, the buckling of MnO_5 bipyramids plays a key role for the formation of FE polarization,[13] giving rise to coupled AFM and FE domains.[38] Similarly, coupled magnetic and electric domains could also present in CFTO, since the magnetic Fe^{2+} ions participate in magnetic and FE orders both. However, the electric polarization of $Sr_{1-x}Ba_xMnO_3$, $Ca_3Mn_2O_7$, and $YMnO_3$ cannot be tuned by external magnetic fields owing to the robust AFM structure.[15–17] In contrast, in the current CFTO, the ground-state AFM spin alignment can be easily changed toward FM correlations, leading to field readily tunable FM domains and relevant FE domains, which is responsible for the unprecedented realization of a magnetic-field controllable displacement-type ferroelectricity. Moreover, when a triangularly periodic magnetic field is applied to CFTO, reproducible variation of the polarization can be observed without any noticeable decay in its magnitude, as illustrated in Figure 5d. Such a well repeatable feature reveals the switchable "On/Off" behavior, providing potential applications in field-controlled electronic devices.

3. Conclusion

In summary, a high-quality quadruple perovskite oxide CFTO was prepared using high-pressure and high-temperature methods. The compound undergoes a displacement-type FE phase transition at 107 K involving considerable off-center displacement of Fe^{2+} ions, giving rise to a structural phase transition from the centrosymmetrical *Im*-3 to a polar *R*3 structure. As the temperature decreased to 3.1 K, the A′-site Fe^{2+} ions experienced a long-range AFM order. Moreover, the AFM ground state is sensitive to an external magnetic field, and a moderate field of ≈0.8 T can induce a metamagnetic phase transition toward the formation of FM corrections. Because the magnetic Fe^{2+} ions simultaneously participate in ferroelectric and spin orders, the magnetic and electric domains are closely coupled with each other. As a result, a large magnetic-field controllable displacement-type polarization with a strong ME coupling effect is realized for the first time. This study provides a prototype material system to realize significant ME coupling effects in displacement-type ferroelectrics with promising applications in advanced electronic devices.

4. Experimental Section

Material Synthesis: Polycrystalline $CaFe_3Ti_4O_{12}$ was synthesized via a solid-state reaction under high-pressure and high-temperature conditions.

Highly pure (>99.9%) CaO, Fe, Fe_2O_3, and TiO_2 powders were used as starting materials. The finely mixed reactants with stoichiometric compositions were packed into a platinum capsule with 3.0 mm diameter and length and then treated at 9 GPa and 1473 K for 1 h on a cubic-anvil-type high-pressure apparatus. During the synthesis, we also attempted to use the precursors $CaTiO_3$ and $FeTiO_3$ as the reactants. However, this method always produces some impurities (≈5 wt.%), as reported in the literatures.[39–41]

Structural and Physical Property Measurements: Synchrotron X-ray diffraction was performed using a Swiss Light Source with a wavelength of 0.56353 Å. The GSAS program[42] was used to refine the structural parameters using the Rietveld full profile refinement method. X-ray absorption spectroscopy measurements were performed at the TLS11A beamline at the Taiwan National Synchrotron Research Center at room temperature. Neutron powder diffraction was performed at the high-resolution powder neutron diffractometer HRPT of Paul Scherrer Institute with a wavelength of 1.494 Å. The temperature dependence of the magnetic susceptibility and the field dependence of the magnetization were measured using a superconducting quantum interference device magnetometer (Quantum Design, MPMS3). Specific heat data were collected using a physical property measurement system (Quantum Design, PPMS-9T). A polished hard disk-shaped pellet (diameter, 2.0 mm) with a thickness of 0.25 mm was used for electric measurements. Frequency-dependent permittivity measurements were performed by using an Agilent-4980A LCR meter in the 2–200 K temperature range. Ferroelectric hysteresis loops were measured at 50 Hz using a Radiant Precision Premier-II Ferroelectric Test System based on the PUND method. Pyroelectric and magnetoelectric currents were recorded using a Keithley 6517 B electrometer. The change in ferroelectric polarization was calculated using the formula $\Delta P\ (t) = P(t) - P\ (0) = \int_0^t I(t)dt/S$, where P denotes the polarization, I denotes the current, t denotes the time, and S denotes the area of the disk-shaped pellet. Before the measurements, the sample was poled with a poling field $E_p = 1$ MV m^{-1}, and 1 h was allowed to pass after removing E_p

First-Principles Calculations: First-principles calculations were carried out using the full-potential linearized augmented plane-wave method as implemented in the WIEN2k package,[43] with the lattice parameters and atomic positions given by the experiment. The muffin-tin radii were set to 2.26 a.u. for Ca, 1.94 a.u. for Fe, 1.79 a.u. for Ti, and 1.62 a.u. for O. A maximum modulus of reciprocal vectors was chosen such that $R_{MT}K_{max} = 8.0$. The Perdew-Burke-Ernzerhof-type generalized-gradient approximation (GGA) was used for the exchange-correlation potential,[44] with 1000 k-points meshes for the whole Brillouin zone and an effective Coulomb interaction $U = 3$ eV for Fe in the GGA+U calculations.[45]

Supporting Information

Supporting Information is available from the Wiley Online Library or from the author.

Acknowledgements

This study was supported by the Beijing Natural Science Foundation (Grant No. Z200007), National Key R&D Program of China (Grant No. 2021YFA1400300), National Natural Science Foundation of China (Grant Nos. 11934017, 12261131499, 11921004, 22271309, and 12204516), and Chinese Academy of Sciences (Grant No. XDB33000000). Z.L. acknowledges the support from the China Postdoctoral Innovative Talent program. The authors acknowledge the Paul Scherrer Institut, Villigen, Switzerland for provision of synchrotron radiation beamtime at beamline MS-Powder of the SLS and would like to thank Dr. Antonio Cervellino for assistance. The authors acknowledge the support from the Max Planck-POSTECH-Hsinchu Center for Complex Phase Materials.

Conflict of Interest

The authors declare no conflict of interest.

Data Availability Statement

The data that support the findings of this study are available from the corresponding author upon reasonable request.

Keywords

A-site ordered perovskite, displacement-type ferroelectric, high-pressure synthesis, magnetoelectric coupling

Received: June 25, 2024
Revised: July 28, 2024
Published online:

[1] M. J. Pan, C. A. Randall, *IEEE Electr Insul Mag* **2010**, *26*, 44.
[2] H. JAFFE, *J. Am. Chem. Soc.* **1958**, *41*, 494.
[3] G. H. Haertling, *J. Am. Ceram. Soc.* **1999**, *82*, 797.
[4] N. A. Hill, *J. Phys. Chem. B* **2000**, *104*, 6694.
[5] R. E. Cohen, *Nature* **1992**, *358*, 136.
[6] R. Seshadri, N. A. Hill, *Chem. Mater.* **2001**, *13*, 2892.
[7] Y.u. F. Popov, A. M. Kadomtseva, S. S. Krotov, D. V. Belov, G. P. Vorob'ev, P. N. Makhov, A. K. Zvezdin, *Low Temp. Phys.* **2001**, *27*, 478.
[8] T. Kimura, S. Kawamoto, I. Yamada, M. Azuma, M. Takano, Y. Tokura, *Phys. Rev. B.* **2003**, *67*, 180401.
[9] Y. Yang, J.-M. Liu, H. B. Huang, W. Q. Zou, P. Bao, Z. G. Liu, *Phys. Rev. B.* **2004**, *70*, 132101.
[10] K. F. Wang, J. M. Liu, Z. F. Ren, *Adv. Phys.* **2009**, *58*, 321.
[11] D. I. Khomskii, *Physics* **2009**, *2*, 20.
[12] D. I. Khomskii, *J. Magn. Magn. Mater.* **2006**, *306*, 1.
[13] B. B. Van Aken, T. T. M. Palstra, A. Filippetti, N. A. Spaldin, *Nat. Mater.* **2004**, *3*, 164.
[14] H. Sakai, J. Fujioka, T. Fukuda, D. Okuyama, D. Hashizume, F. Kagawa, H. Nakao, Y. Murakami, T. Arima, A. Q. R. Baron, Y. Taguchi, Y. Tokura, *Phys. Rev. Lett.* **2011**, *107*, 137601.
[15] M. Liu, Y. Zhang, L.-F. Lin, L. Lin, S. Yang, X. Li, Y.u Wang, S. Li, Z. Yan, X. Wang, X.-G. Li, S. Dong, J.-M. Liu, *Appl. Phys. Lett.* **2018**, *113*, 022902.
[16] F. Kadlec, V. Goian, C. Kadlec, B. Dabrowski, D. Nuzhnyy, M. Kempa, V. Bovtun, M. Savinov, J. Hejtmánek, J. Prokleška, S. Kamba, in *41st International Conference on Infrared, Millimeter, and Terahertz Waves (IRMMW-THz)*, Copenhagen, Denmark, **2016**.
[17] Z. J. Huang, Y. Cao, Y. Y. Sun, Y. Y. Xue, C. W. Chu, *Phys. Rev. B.* **1997**, *56*, 2623.
[18] R.-E. Patru, C. A. Stanciu, E. M. Soare, V.-A. Surdu, R. D. Trusca, A. I. Nicoara, B. S. Vasile, G. Boni, L. Amarande, N. Horchidan, L. P. Curecheriu, L. Mitoseriu, L. Pintilie, I. Pintilie, A.-C. Ianculescu, *J. Eur. Ceram. Soc.* **2023**, *43*, 3250.
[19] D. G. Tomuta, S. Ramakrishnan, G. J. Nieuwenhuys, J A. Mydosh, *J. Phys.: Condens. Matter.* **2001**, *13*, 4543.
[20] S. Lee, A. Pirogov, M. Kang, K.-H. Jang, M. Yonemura, T. Kamiyama, S.-W. Cheong, F. Gozzo, N. Shin, H. Kimura, Y. Noda, J.-G. Park, *Nature* **2008**, *451*, 805.
[21] K. Cho, S. Hur, S. Park, *Appl. Phys. Lett.* **2017**, *110*, 162905.
[22] M. Fukunaga, Y. Noda, *J. Phys. Soc. Japan.* **2008**, *77*, 064706.
[23] S. M. Feng, Y. S. Chai, J. L. Zhu, N. Manivannan, Y. S. Oh, L. J. Wang, Y. S. Yang, C. Q. Jin, K. H. Kim, *New J. Phys.* **2010**, *12*, 073006.
[24] M. V. Talanov, *Acta Cryst. A* **2019**, *75*, 379.
[25] H. T. Stokes, D. M. Hatch, *Isotropy subgroups of the 230 crystallographic Space Groups*, World Scientific, Singapore, **1988**.
[26] W. J. Merz, *Phys. Rev.* **1953**, *91*, 513.
[27] M. A. Subramanian, D. Li, N. Duan, B. A. Reisner, A. W. Sleight, *J. Solid State Chem.* **2000**, *151*, 323.

[28] J. Kumar, R. J. Choudhary, A. M. Awasthi, *Appl. Phys. Lett.* **2014**, *104*, 262905.
[29] M. Amano Patino, F. Denis Romero, H.-J. Koo, M. Avdeev, S. D. A. Injac, M. Goto, M.-H. Whangbo, Y. Shimakawa, *Commun. Mater.* **2022**, *3*, 51.
[30] K. Shiro, I. Yamada, N. Ikeda, K. Ohgushi, M. Mizumaki, R. Takahashi, N. Nishiyama, T. Inoue, T. Irifune, *Inorg. Chem.* **2013**, *52*, 1604.
[31] J. Zhao, J. Gao, W. Li, Y. Qian, X. Shen, X. Wang, X.i Shen, Z. Hu, C. Dong, Q. Huang, L. Cao, Z. Li, J. Zhang, C. Ren, L. Duan, Q. Liu, R. Yu, Y. Ren, S.-C. Weng, H.-J.i Lin, C.-T.e Chen, L.-H. Tjeng, Y. Long, Z. Deng, J. Zhu, X. Wang, H. Weng, R. Yu, M. Greenblatt, C. Jin, *Nat. Commun.* **2021**, *12*, 747.
[32] N. A. Benedek, C. J. Fennie, *J. Phys. Chem. C.* **2013**, *117*, 13339.
[33] J. B. Goodenough, *Rep. Prog. Phys.* **2004**, *67*, 1915.
[34] S.-W. Cheong, M. Mostovoy, *Nat. Mater.* **2007**, *6*, 13.
[35] N. Hur, S. Park, P. A. Sharma, J. S. Ahn, S. Guha, S.-W. Cheong, *Nature* **2004**, *429*, 392.
[36] T. Kimura, T. Goto, H. Shintani, K. Ishizaka, T. Arima, Y. Tokura, *Nature* **2003**, *426*, 55.
[37] G. Lawes, A. B. Harris, T. Kimura, N. Rogado, R. J. Cava, A. Aharony, O. Entin-Wohlman, T. Yildirim, M. Kenzelmann, C. Broholm, A. P. Ramirez, *Phys. Rev. Lett.* **2005**, *95*, 087205.
[38] M. Fiebig, T.h. Lottermoser, D. Fröhlich, A. V. Goltsev, R. V. Pisarev, *Nature* **2002**, *419*, 818.
[39] M. Amano Patino, F. Denis Romero, M. Goto, T. Saito, F. Orlandi, P. Manuel, A. Szabó, P. Kayser, K.a H. Hong, K. N. Alharbi, J. P. Attfield, Y. Shimakawa, *Phys. Rev. Res.* **2021**, *3*, 043208.
[40] K. Leinenweber, J. Linton, A. Navrotsky, Y. Fei, J. B. Parise, *Phys. Chem. Miner.* **1995**, *22*, 251.
[41] J. Linton, A. Navrotsky, Y. Fei, *Phys. Chem. Miner.* **1998**, *25*, 591.
[42] B. H. Toby, *J. Appl. Crystallogr.* **2001**, *34*, 210.
[43] P. Blaha, K. Schwarz, G. K. H. Madsen, D. Kvasnicka, J. Luitz, *WIEN2k, An Augmented Plane Wave Plus Local Orbitals Program for Calculating Crystal Properties*, Vienna University of Technology, Austria **2001**.
[44] J. P. Perdew, K. Burke, M. Ernzerhof, *Phys. Rev. Lett.* **1996**, *77*, 3865.
[45] D. Huang, Y. Pan, *High Pressure Res.* **2012**, *32*, 270.